Theoretical and Experimental Investigation of the Dynamics of the Production of CO from the $CH_3 + O$ and $CD_3 + O$ Reactions

Timothy P. Marcy, Robert Richard Díaz,[†] Dwayne Heard,[‡] and Stephen R. Leone*[,§]

JILA, National Institute of Standards and Technology and University of Colorado, and Department of Chemistry and Biochemistry, University of Colorado, Boulder, Colorado 80309-0440

Lawrence B. Harding*

Chemistry Division, Argonne National Laboratory, Argonne, Illinois 60439-4803

Stephen J. Klippenstein*

Combustion Research Facility, Sandia National Laboratories, Livermore, California 94551-0969

Received: March 15, 2001; In Final Form: June 19, 2001

Combined experimental and theoretical investigations of the title reactions are presented. Time-resolved Fourier transform infrared (FTIR) emission studies of CO ($v = 1$) produced from the $CH_3 + O$ and $CD_3 + O$ reactions show that there is approximately a one-third reduction in the branching to the CO channel upon deuteration of the methyl radical. Direct dynamics, classical trajectory calculations using a B3LYP potential surface, confirm the existence of the CO producing channel. The calculations show that the CO comes from the decomposition of HCO produced by the elimination of H_2 from highly vibrationally excited methoxy radicals. Scans of the potential surface reveal no saddle point for the direct elimination of H_2 from methoxy. The minimum-energy path for this elimination is a stepwise process involving first a CH bond cleavage, forming $H + H_2CO$, followed by an abstraction, forming $H_2 + HCO$. However, at the high internal energies produced in the initial $O + CH_3$ addition, trajectories for the direct elimination of H_2 from methoxy are observed. The predicted branching ratio between the CO and H_2CO channels is in good agreement with previous room-temperature measurements, and there is predicted to be little temperature dependence to it. The observed reduction in the branching to the CO channel upon deuteration is also well reproduced in the calculations.

Introduction

The reaction of methyl radicals with oxygen atoms is an important reaction in the combustion of small hydrocarbons. It is an important pathway for the removal of methyl radicals, particularly under lean fuel conditions. Although there are six possible sets of exothermic products for this reaction

$$CH_3 + O \rightarrow H + H_2CO \qquad \Delta H = -70 \text{ kcal/mol} \qquad (1a)$$

$$\rightarrow H_2 + HCO \qquad \Delta H = -84 \qquad (1b)$$

$$\rightarrow H + HCOH \qquad \Delta H = -13 \qquad (1c)$$

$$\rightarrow H_2 + COH \qquad \Delta H = -44 \qquad (1d)$$

$$\rightarrow H + H_2 + CO \qquad \Delta H = -70 \qquad (1e)$$

$$\rightarrow CH + H_2O \qquad \Delta H = -10 \qquad (1f)$$

(where 1 kcal/mol = 4.18 kJ/mol), it was long assumed that the only products are formaldehyde and atomic hydrogen. However, in 1992, Seakins and Leone[1] reported the detection of CO (v) from this reaction using FTIR emission spectroscopy, and they estimated the CO branching fraction to be 0.40 ± 0.10. More recently, Fockenberg et al.[2] have reported a time resolved, time-of-flight mass spectroscopic study of this reaction that yielded a room-temperature branching ratio of 0.17 ± 0.11 for the formation of CO, while their subsequent infrared diode laser spectroscopy experiment yielded a branching ratio of 0.18 ± 0.04.[3] Min et al.[4] have also confirmed the production of vibrationally excited CO in this reaction.

The presumed mechanism for this reaction is as follows:

$$CH_3 + O \rightarrow H_3CO^* \rightarrow H + H_2CO$$

$$\rightarrow H_2 + HCO^* \rightarrow H_2 + H + CO$$

in which there is an initial addition of the reactants, forming a highly energized methoxy radical intermediate, which can then decompose by CH bond cleavage, forming formaldehyde, or by eliminating molecular hydrogen to form HCO. The HCO then undergoes a further decomposition, leading to the observed product, CO. A puzzling aspect of this mechanism is that although attempts have been made to locate a transition state for the elimination of molecular hydrogen from methoxy radical, none have been found. Note that the alternative, in which CO is formed by the elimination of H_2 from formaldehyde formed in reaction 1a, is not energetically feasible due to the large barrier for $H_2CO \rightarrow H_2 + CO$.

* Corresponding authors.
[†] NSF-REU student, Department of Chemistry, University of Puerto Rico, San Juan, Puerto Rico, 00931-3346
[‡] JILA Visiting Fellow. Permanent address: School of Chemistry, University of Leeds, Leeds, LS2 9JT, England.
[§] Staff Member, Quantum Physics Division, National Institute of Standards and Technology.

10.1021/jp010961f CCC: $20.00
Published on Web 08/17/2001

In this paper, we report (1) a new time-resolved, Fourier transform infrared emission spectroscopic study of the title reactions, (2) a detailed, ab initio characterization of the CH_3O potential surface, and (3) a direct dynamics study of the title reactions using classical trajectories and a B3LYP/6-31G* potential surface. The goal of this study is to understand the mechanism for the production of CO (v) and factors that control the branching between CO (v) and H_2CO.

Experimental Section

Experimental Methods. The CO (v) produced by the reaction CH_3 or $CD_3 + O$ is studied by time-resolved Fourier transform infrared (FTIR) emission spectroscopy.[5−7] This technique allows simultaneous observation of the time evolution of a number of spectral features that correspond to different quantum states of the CO (v) products of the reaction, as well as the H_2CO (v) or D_2CO (v) products.

Since the apparatus is described in detail elsewhere[8] only a brief summary is presented here. The reactant radicals are created by 193 nm laser flash photolysis of SO_2 and either acetone or d_6-acetone precursor molecules; this yields $O(^3P)$ atoms and either CH_3 or CD_3 radicals. The laser energy in the chamber is approximately 30 mJ/pulse with a 1 cm^2 beam profile. The generation of the reactant radicals initiates the reaction. The photolysis of acetone also directly produces CO (v). The precursor gases are mixed in an effusive source upstream from the photolysis laser. Both the acetone vapor, from a room-temperature flask of the liquid, and the SO_2 are metered into the reaction chamber by needle valves. Conditions are chosen such that the SO_2/acetone density ratio is ∼3:1, which, when cross sections at 193 nm are taken into account, gives the O/CH_3 and O/CD_3 ratios of ∼9:2 and ∼3:1, respectively. The continuous flow of precursor gases is confined to the photolysis region by a background of ∼50 Pa of argon. All of the gases are exhausted from the chamber by a 300 L/s pump. The absolute concentrations of the reactants in this experiment are not well-defined, as the reaction region is situated between the source and sink of the gases and direct measurement is not feasible. The densities can be estimated to be on the order of 10^{15} radicals/cm^3 using the known[2] rate constant of 1.7×10^{-10} cm^3 $molecule^{-1}$ s^{-1} for the $CH_3 + O$ reaction and fitting our observed rise times.

Emission from excited products of both photolysis and reaction is collected by Welsh cell optics in the chamber and focused by CaF_2 lenses into a commercial step-scan FTIR spectrometer.[9] Time resolution is achieved by operating the spectrometer in the step-scan mode. The interferometer mirror is stepped through its range, being fixed at each position while a full time history of the reaction for ∼200 coadded laser pulses is obtained. Once all of the mirror positions are sampled, the data at each time are used to construct interferograms, which are then Fourier transformed to create spectra at each time. The spectral resolution for all of the spectra presented here is 0.6 cm^{-1}, and the time interval between spectra is 2.5 μs.

Since the photolysis of acetone itself produces CO (v), the emission is distinguished from the CO (v) produced by the reaction of interest by obtaining spectra from the photolysis of acetone in the absence of SO_2. These spectra are then subtracted from the spectra of emission from CO (v) that is produced both by the reaction and acetone photolysis with SO_2 present.

Identical experimental conditions, including equal concentrations of deuterated and nondeuterated acetone and SO_2, minimize the variations between the experiments, although as noted below, the cross sections for acetone photolysis at 193 nm differ significantly for the deuterated and nondeuterated species.

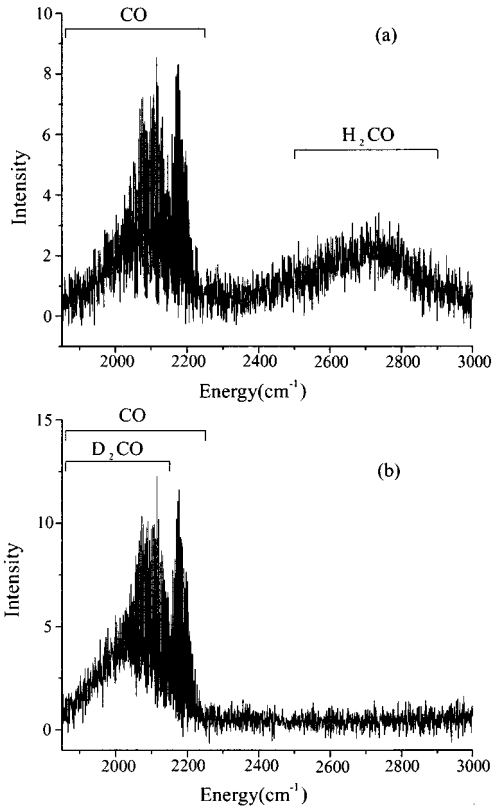

Figure 1. Emission spectra from the products of the reaction of $O(^3P)$ with (a) CH_3 and (b) CD_3, at 0.6 cm^{-1} resolution. Emission from CO ($\Delta v = -1$) appears from 2250 to the 1850 cm^{-1} detection limit of the infrared detector. Emission from H_2CO appears between approximately 2500 and 2900 cm^{-1}, while the D_2CO emission overlaps the CO emission below 2150 cm^{-1}.

Experimental Results. Figure 1 shows FTIR emission spectra obtained from the products of the photolysis of a mixture of SO_2 with either (a) acetone or (b) deuterated acetone. Emission from the $\Delta v = -1$ sequence bands of CO arises both from the reaction of the CH_3 or CD_3 with $O(^3P)$ photofragments and from the direct photolysis of the acetone. The H_2CO or D_2CO emission comes solely from the reaction and is not rotationally resolved. Because of the isotopic shift of the D_2CO, its emission overlaps the CO (v) emission, as seen in Figure 1b, which complicates the analysis of the CO spectrum in the deuterated experiments. While this overlap prevents an accurate determination of the CO (v) vibrational distribution from the $CD_3 + O$ reaction, the spectra in Figure 1 indicate that the distribution is qualitatively similar to that from the $CH_3 + O$ reaction, suggesting that the mechanisms that produce the CO (v) are similar in each case.

To deconvolute the emission from CO (v) produced by the reaction from that produced by direct photolysis, spectra of CO (v) emission from the photolysis of acetone alone are acquired, with the acetone concentration the same as in the reaction experiments. A small wavelength range of each acetone photolysis-only spectrum (acetone and d_6-acetone) is shown in Figure 2, along with spectra that also include the reaction. The differences between these spectra are the emissions from the CO (v) produced by the reactions.

The portion of the spectrum shown in Figure 2 is the rotationally resolved R-branch of CO ($v = 1$), chosen because there is no interference from D_2CO in this region. The fairly smooth Boltzmann distribution of intensities of the rotational lines of the CO produced solely by photolysis shows that it is approximately in thermal equilibrium with a temperature of 300

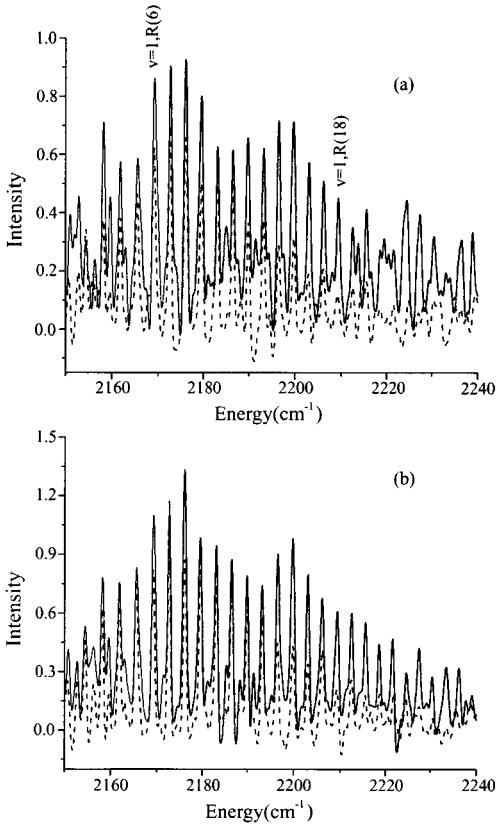

Figure 2. (a) Emission spectra of the R-branch of CO ($v = 1$) produced from the photolysis of acetone with SO_2 (—) and from the photolysis of acetone alone (- - -). (b) Emission spectra of CO ($v = 1$) produced from photolysis of d_6-acetone with SO_2 (—) and from d_6-acetone alone (- - -). The difference between the solid and dotted spectra is the CO (v) emission from the CH_3 or CD_3 + O reaction.

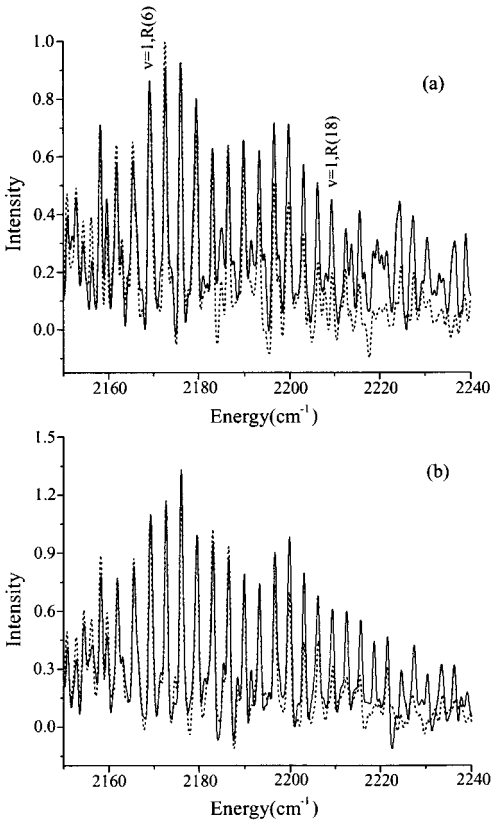

Figure 3. Emission spectra of CO ($v = 1$) produced from the reaction of O + (a) CH_3 and (b) CD_3 at 10 μs (—) and 90 μs (·····) after the reaction is initiated. The bimodal rotational distribution of CO ($v = 1$) relaxes with time.

K. This is expected because these spectra (an average of four spectra for improved signal-to-noise) are acquired between 5 and 15 μs after photolysis, corresponding to about 30 collisions, which appears to be sufficient, by comparison to the data at different time delays, to equilibrate the rotational distributions if the CO was initially hot. In contrast, the spectra that include emission from the reaction products, also shown in Figure 2, have bimodal rotational distributions with second intensity maxima near 2200 cm^{-1} for both the acetone and d_6-acetone precursors. This indicates that rotationally hot CO (v) is produced by reaction sufficiently quickly (presumably from the dissociation of a bent HCO transient species) to compete with collisional deactivation. Figure 3 compares these reaction spectra (5−15 μs) with spectra obtained between 85 and 95 μs after photolysis. This comparison shows a reduction in relative intensity of the lines near 2200 cm^{-1} and above, indicating that the rotational distribution approaches equilibrium at later times as the rate of production of the hot product decreases. The CO (v) molecules produced from both the deuterated and non-deuterated reactants show similar behavior.

To compare the relative yields of CO (v) produced by the two reactions (CH_3 and CD_3 with O), experiments are performed under identical conditions and precursor concentrations in each case. We analyze only the CO ($v = 1 \rightarrow 0$) band because of the interference of D_2CO emission below 2150 cm^{-1} and because too few rotational lines are resolved in the higher vibrational states to make an accurate comparison without knowing the rotational distributions. Comparison of the photolysis-only spectra in Figure 2 shows that the deuterated species produces 1.5 ± 0.2 times more CO ($v = 1$). The ratio is obtained by summing over the R-branch lines of sufficient intensity for accurate measurement: $J = 6-18$. These lines include both maxima in the bimodal rotational distribution of the reaction spectra and thus should account for any difference in rotational distribution in the different cases. This ratio is similar to the ratios of absorption cross sections at 193 nm and 300 K of d_6-acetone to acetone. We have measured the cross-section ratio at 193 nm in two ways. The result using a commercial UV−visible spectrometer is 1.5 ± 0.1. Monitoring the change in power of the excimer laser used in the FTIR experiments transmitted through the chamber filled with acetone with static pressures varied between 7 and 40 Pa yields a ratio of 1.4 ± 0.1. The ratio has previously been measured by a similar laser transmittance method to be 1.29 ± 0.05.[10] The amount of CO produced from the 193 nm photolysis of acetone should be proportional to the amount of CH_3 or CD_3 produced. We take the 1.5 ± 0.2 ratio of the CO (v) yields to be the most direct measure of the ratio of CD_3 to CH_3 produced and available for reaction and use this value for calculation of the results that follow.

The amount of CO (v) produced by photolysis is subtracted from the data obtained with SO_2, and the resulting reaction yields are normalized for this 1.5± 0.2 ratio of reactant concentrations. This analysis shows that only 69 ± 10% as much CO ($v = 1$) is produced per CD_3 as per CH_3 radical (with the experimental uncertainty propagated from 1σ baseline noise in the data). Since the vibrational distribution of the CO produced from the deuterated reaction is not precisely known, the ratio of the total CO (v) produced in the two reactions may differ somewhat from that of CO ($v = 1$), especially since CO (v) up to $v = 8$ is expected.[1] The difference in CO ($v = 1$) is likely attributed to a change in the branching ratios of H_2CO/CO (v

$= 1$) versus D_2CO/CO ($v = 1$) for $CH_3 + O$ and $CD_3 + O$, respectively, but could be due to changes among CO (v) populations.

The above measurements are made at early times, 5−15 μs after laser initiation of the reaction, so errors due to different CO (v) deactivation rates due to different precursor gases present are not significant. Comparison of the reaction signal at this early time will be valid only if the rates of production of CO (v) from the reaction of $CH_3 + O$ and $CD_3 + O$ are similar. To our knowledge, the rate constant for the $CD_3 + O$ reaction has not been measured. Complications due to the overlap of the D_2CO and CO emission and vibrational cascading of the CO prevent the accurate extraction of the relative rates from our data, although such experiments were attempted. However, we expect that deuteration of the methyl radical will have little effect on the rate coefficients. The barrierless association of the two radicals yields a complex with energy much higher than the barriers to H atom or H_2 elimination, so the association is expected to be the rate-determining step in the process while not being strongly affected by deuteration. In the case that the rates are similar, the comparison of the CO ($v = 1$) yield at early times shows that the effect of the deuterated isotope reactant on the $CH_3 + O$ reaction is to reduce the yield of CO ($v = 1$) by one-third. Presuming that the CO ($v = 1$) yield is indicative of the entire CO (v) population, the branching fraction to the CO (v) product is decreased by deuteration of CH_3.

Theoretical Section

Electronic Structure Methods. The present study employs two kinds of electronic structure methods, the density functional, B3LYP, and the coupled cluster, singles and doubles with perturbative triples, CCSD(T). The B3LYP calculations were carried out with the GAUSSIAN98 program[11] using the 6-31G* basis set. To check the accuracy of the B3LYP calculations, CCSD(T) calculations[12] were done using the MOLPRO program.[13] CCSD(T) geometry optimizations and normal-mode analyses were performed using the Dunning[14−16] cc-pvdz basis set. Single point calculations were then done using the larger aug-cc-pvtz basis set at the CCSD(T)/cc-pvdz geometries.

Electronic Structure Results. The calculated energies of the stationary points on the CH_3O potential surface are listed in Table 1 and shown schematically in Figure 4. Overall, there is reasonable agreement between the B3LYP/6-31G*, CCSD(T)/aug-cc-pvtz and (where available) experimental results. This agreement validates the use of the B3LYP/6-31G* method in the present direct dynamics study. Various aspects of these energetics have been examined in prior theoretical studies, with the most accurate of those being the internally contracted configuration interaction (ICCI) study of Walch.[17] Where the two studies overlap, there is good agreement (2 kcal/mol or better) between the present CCSD(T)/aug-cc-pvtz results and the ICCI results of ref 17.

The CCSD(T)/aug-cc-pvtz calculations consistently underestimate, by ~4 kcal/mol, the energies of species having a CO bond relative to the reactants $CH_3 + O$. Most of this error can be traced to the basis set. For example, the CCSD(T) exothermicity of the reaction $CH_3 + O \rightarrow H_2 + H + CO$ is underestimated by 3.4, 3.1, and 1.0 kcal/mol, respectively with the cc-pvdz, aug-cc-pvtz, and aug-cc-pvqz basis sets. The errors in the DFT calculations, although comparable in magnitude to the CCSD(T)/aug-cc-pvtz results, are less consistent. For example, the errors in the energies of CH_3O and H_2COH relative to $CH_3 + O$ are +3.7 and +4.2 kcal/mol, respectively, with CCSD(T)/aug-cc-pvtz and −1.9 and +5.9 kcal/mol, respectively, with B3LYP/6-31G*.

TABLE 1: Relative Energies (kcal/mol, including zero point) for the Stationary Points on the CH_3O Potential Surface

	B3LYP/ 6-31G*	CCSD(T)/ cc-pvdz	CCSD(T)/ aug-cc-pvtz[a]	exp't
$CH_3 + O$	0.0	0.0	0.0	0.0[d]
CH_3O	−90.6	−76.5	−85.0	−88.7[e]
H_2COH	−91.3	−81.8	−93.0	−97.2[e,f]
$HCOH_2$	−9.7	−8.5	−17.1	
$H + H_2CO$	−65.8	−59.7	−65.1	−69.8[d]
H + HCOH (trans)	−8.7	−7.4	−13.5	
H + HCOH (cis)	−4.2	−3.2	−9.2	
$H_2 + HCO$	−83.7	−75.7	−81.2	−84.3[e]
$H_2 + COH$	−38.9	−34.1	−40.1	
$H + H_2 + CO$	−63.4	−66.8	−67.1	−70.2[d]
$CH(^2\Pi) + H_2O$	5.3	2.0	−9.0	−10[d]
$CH_3O \rightarrow H + H_2CO$	−63.4	−51.9	−59.9	
$H_2COH \rightarrow H + H_2CO$	−59.7	−45.5	−52.8	
$CH_3O \rightarrow H_2COH$	−55.5	−43.6	−55.1	
$H_2COH \rightarrow HCOH_2$	−4.1	−0.3	−9.3	
$H + H_2CO \rightarrow H_2 + HCO$	−66.0	−53.9	−59.4	
$H_2COH \rightarrow H_2 + COH$	−2.2	2.8	−7.2	
H_2COH - internal rotation	−87.7	−77.9	−89.6	
$H_2CO \rightarrow H_2 + CO$	18.4[b]	21.1[b]	16.4[b]	
$H_2CO \rightarrow HCOH$ (trans)	21.3[b]	23.7[b]	17.0[b]	
$COH \rightarrow H + CO$	−37.3[c]	−29.1[c]	−34.1[c]	
$HCO \rightarrow H + CO$	−66.3[c]	−61.1[c]	−63.3[c]	

[a] Using CCSD(T)/cc-pvdz geometries and zero point. [b] Energy of TS plus energy of H atom. [c] Energy of TS plus energy of H_2 molecule. [d] Chase, M. W., Jr. *NIST-JANAF Thermochemical Tables*, 4ed.; *J. Phys. Chem. Ref. Data* **1998**, Monograph No. 9. [e] Berkowitz, J.; Ellison, G. B.; and Gutman, D. *J. Phys. Chem*. **1994**,*98*, 2744. [f] M. Litorja, Ruscic, B. *J. Electron Spectrosc. Relat. Phenom.* **1998**, *97*,131.

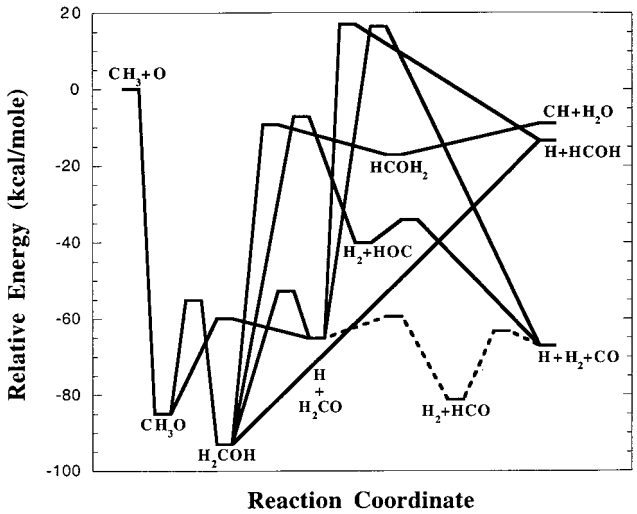

Figure 4. Schematic of the stationary point energies on the CH_3O potential surface. The results shown are from CCSD(T)/aug-cc-pvtz//CCSD(T)/cc-pvdz calculations (including zero point).

As noted in the Introduction, no saddle point could be found for the direct elimination of H_2 from CH_3O. If two of the CH bond lengths are constrained to be of equal length, a direct pathway for elimination of H_2 can be found with a barrier of ~50 kcal/mol at the CCSD(T)/cc-pvdz level. Note that this is still ~30 kcal/mol below the reactants, $CH_3 + O$. However this "barrier" does not correspond to a stationary point in the full nine dimensional coordinate space. Transition state searches started at this point collapse to the saddle point for loss of a hydrogen atom.

An indirect path for elimination of H_2 was found involving first the isomerization of CH_3O to H_2COH, followed by a (1,1) elimination forming $H_2 + HOC$. This process, while predicted

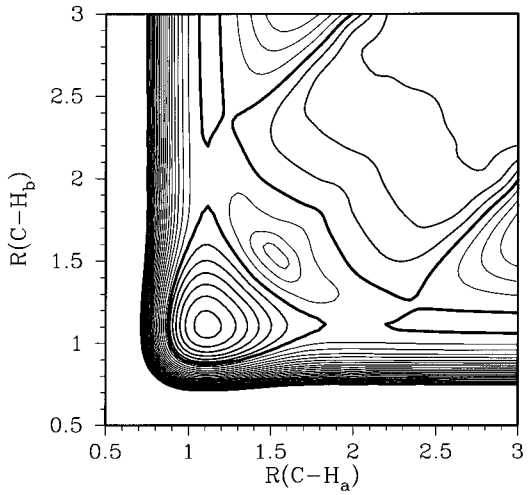

Figure 5. B3LYP/6-31G* energy contours for CH_3O as a function of two of the CH bond lengths. All other geometric parameters are optimized at each point. The darkest contours correspond to the energy of the saddle point for H + $H_2CO \rightarrow H_2$ + HCO. The lightest contours are higher in energy and the darker contours are lower. The contour increment is 5 kcal/mol. The length scales are in Å.

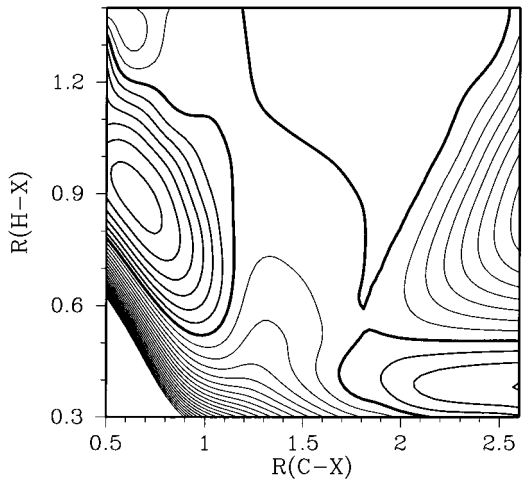

Figure 6. B3LYP/6-31G* energy contours for CH_3O as a function of *R*(X−H) and R(X−C), where X is the midpoint of two of the hydrogens. Other conventions are the same as those for Figure 5.

to be energetically accessible from the reactants, has a much larger barrier than hydrogen atom loss, and no evidence for this process was observed in the direct dynamics calculations described below.

In an attempt to better understand the topology of this potential surface, two reduced dimensional (2D) surfaces were evaluated at the B3LYP/6-31G* level of theory. These surfaces were obtained by constraining two degrees of freedom while optimizing the remaining seven degrees of freedom over a two-dimensional grid. Contour plots of these two surfaces are shown in Figures 5 and 6. In Figure 5, the constrained degrees of freedom are two of the CH bond distances. In Figure 6, the constrained parameters are one of the HH distances and the distance between the carbon atom and the midpoint of these two hydrogens. In Figure 5, four distinct minima and four transition states are visible. The methoxy radical minimum is in the lower left corner. Two symmetry-related valleys, leading to H_a + H_2CO and H_b + H_2CO, lie parallel to the horizontal and vertical axes, respectively. A broad valley leading out to H_aH_b + HCO lies in the upper right corner of the plot. Transition states for H atom elimination can be seen separating the methoxy minimum and the H + H_2CO valleys. Also visible in this plot are two symmetry-related transition states for the abstraction reaction H + $H_2CO \rightarrow H_2$ + HCO. In this plot, direct pathways between methoxy and H_2 + HCO appear to be blocked by the presence of a maximum in the potential at $R(C-H_a) = R(C-H_b) = 1.6$ Å.

Examination of Figure 6 leads to similar conclusions. In this plot, the methoxy minimum is at the center of the left-hand side of the plot, the valley leading to H_2 + HCO is in the lower right, and the valley leading to H + H_2CO is in the top right. Again transition states for $H_3CO \rightarrow$ H + H_2CO and H + $H_2CO \rightarrow H_2$ + HCO can be seen. Here, direct paths from methoxy to H_2 + HCO are blocked by the ridge at $R(C-H_2) = 1.4$ Å. Although Figures 5 and 6 suggest that there is no saddle point for the elimination of H_2 from methoxy, the high dimensionality of this problem precludes a definitive conclusion.

Direct Dynamics Methods. The implementation of a direct dynamics procedure requires the choice of (i) an underlying ab initio methodology, (ii) a procedure for generating initial conditions, (iii) an algorithm for propagating the phase space variables in time, and (iv) a set of conditions for ending the propagations. The particular algorithm employed here is based on that employed in a recent study of the dissociation of CH_2CO.[18]

The B3LYP density functional generally provides a semi-quantitative description of potential surfaces for the majority of configuration space and does so at relatively modest computational cost. The electronic structure results presented above indicate that for the CH_3 + O system the B3LYP/6-31G* method provides an adequate description of at least the energetics of the various stationary points. Thus, the B3LYP/6-31G* method was employed in the present direct dynamics simulations.

Each of the trajectories was initiated on a dividing surface defined by a constant CO separation of 2.65 Å, which roughly corresponds to the expected transition state separation for the initial addition reaction. The remaining variables were sampled with a random sampling analogous to that employed in an algorithm for the evaluation of the number of available states for motion on the dividing surface.[19] This procedure is based on an assumed mode separability into the internal vibrations of the two reacting fragments (termed the conserved modes) and the fragment and orbital rotations and relative translation (termed the transitional modes). First, the coordinates and momenta for the internal vibrational modes are chosen with random vibrational phase and amplitudes corresponding to the zero-point energy in each mode. This conserved mode sampling assumes harmonic behavior for the conserved mode potential. However, the classical anharmonic fragment vibrational energy is easily evaluated via a direct determination of the fragment potential energy for the chosen conserved mode coordinates E^{anh}.

The coupling of this conserved mode sampling with the transitional mode sampling to produce an *E* and *J* resolved sampling may be accomplished in a variety of ways. In particular, one could produce a microcanonical distribution by constraining the energy of the transitional modes to be equal to the total energy *E* minus E^{anh}. However, the considerable variations in E^{anh} would yield undesirable fluctuations in the transitional mode energies. Alternatively, one could renormalize the internal vibrational displacements and/or their conjugate momenta to obtain internal vibrational energy properly equal to the harmonic zero-point energy E_0. The transitional mode energies would then be sampled with constant energy equal to $E - E_0$. However, this procedure would require an iterative

evaluation of the fragment vibrational energy, which was deemed unnecessary. Instead, the present algorithm simply allows the total energy to vary with the variations in the conserved mode energy, and it employs a constant transitional mode energy, again equal to $E - E_0$.

For the $CH_3 + O$ reaction, both the products and the transition states are highly exothermic, and the various modes are strongly coupled in the region of the initial complex. Thus, the dynamics are unlikely to be strongly dependent on minor variations in the initial energy, and so, any of these approaches would be expected to produce similar results. Indeed, only minor differences related to the dynamics of the initial addition process were observed when sample calculations analogous to the first algorithm were performed.

The phase space variables for the transitional modes are sampled randomly within the constraint of constant energy, $E - E_0$, and total angular momentum J according to the algorithm for evaluating the transitional mode number of available states described in ref 19. The neglect of the conserved-transitional mode couplings results in some modest variations in J, as does the neglect of the internal fragment vibrational contributions to J. The neglect of the former also further affects the assumed proportioning between conserved and transitional mode energies.

With this sampling procedure, each initial trajectory i has a weight w_i associated with it, equal to the transition state estimate for the contribution of the corresponding initial configuration to the reactive flux through the dividing surface. Quantities such as the product distributions are then evaluated as a weighted average over the trajectories:

$$P_j = \sum_i w_i \chi_{ij}$$

where χ_{ij} is unity if trajectory i produces product j and zero otherwise.

The trajectories were propagated with the position Verlet method,[20,21] using directly determined analytical B3LYP/6-31G* forces and were terminated when any of the interatomic distances exceeded the threshold of 4.8 Å. A time step of 10 au was generally employed, with the total propagation time typically being between 10^3 and 10^4 au $= 20-200$ fs. During this propagation the total energy is generally conserved to about 1×10^{-4} au. This level of convergence was deemed sufficient for the present primary purpose of searching for the mechanism and determining the distribution between H_2 and H loss channels.

Wave function convergence problems were occasionally encountered with the standard self-consistent field (SCF) algorithm of GAUSSIAN98 during the propagation, with these difficulties arising most commonly during the generation of the initial conditions. These failures were simply remedied via a temporary switch to a quadratically convergent SCF algorithm.

Direct Dynamics Results. The propagation of 240 $CH_3 + O$ trajectories at an initial transitional mode energy of 0.005 au and $J = 50$ yields an $H_2 + HCO$ branching fraction of 0.140 ± 0.028. The only other product observed was $H + H_2CO$. Nineteen trajectories sampled the H_2COH well, and 10 trajectories redissociated back to reactants. More limited propagations with $J = 0$, 30, 70, and 100, and for the same transitional mode energy, yield the $H_2 + HCO$ branching fractions shown in Figure 7. From this plot, it can be seen that the branching ratio peaks at intermediate J and falls off both for low and high J.

Because of the great exothermicity of the pathways connecting the initial CH_3O adduct with the two observed products, this branching fraction is expected to be at most only weakly dependent on E, and so, this dependence is not considered here. This exothermicity should also lead to the immediate further dissociation of the HCO product into $H + CO$. In the absence of any energy dependence for the branching ratio, one can obtain an estimate for the temperature dependence of the branching ratio by coupling the J dependent predictions with an estimate for the temperature dependence of the distribution of J produced in the initial association process. Here these initial J distributions are obtained from model variational transition state theory calculations designed to reproduce the known reaction rate constant.[22]

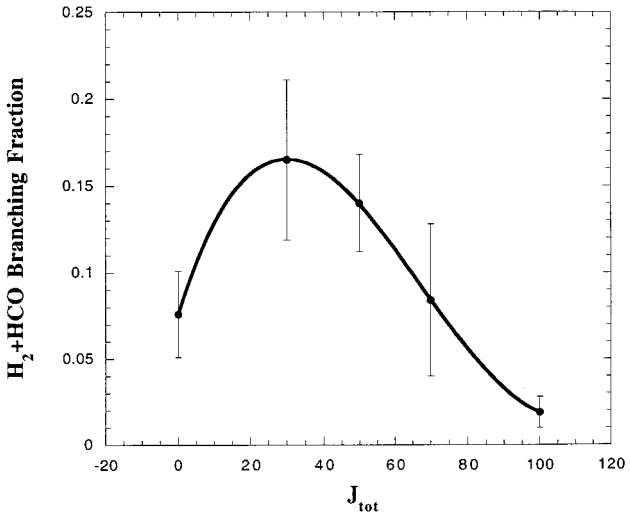

Figure 7. $H_2 + HCO$ branching ratio as a function of J. The solid curve is a cubic fit to the calculated points.

Remarkably, the resulting prediction of 0.15 for the room-temperature branching ratio is within the error bars of the most precise experimental measurement of 0.18 ± 0.04.[3] This predicted branching ratio falls slightly with temperature, reaching a value of 0.13 at 1000 K. While there may be some modest energy dependence on the branching ratio, particularly for the higher J values where the available energy at the transition state is considerably reduced, it is unlikely to result in a strong temperature dependence.

The equivalent propagation of 200 trajectories for $CD_3 + O$, again at a transitional mode energy of 0.005 au and $J = 50$, yielded a branching ratio of 0.086 ± 0.021. Also, sample variational transition state theory calculations indicate that the difference between the J distributions produced in the $CD_3 + O$ and $CH_3 + O$ reactions is not large enough to produce a significant difference in the predicted thermal branching ratios. Thus, to a first approximation, the theoretically predicted branching ratio for the CD_3 reaction should be reduced by a factor of 0.61, in quantitative agreement with the present experimental observations of only $^2/_3$ as much population in CO ($v = 1$) for $CD_3 + O$ as compared to that for $CH_3 + O$. Overall, these direct trajectories provide a strong confirmation of the presence of a significant amount of a CO producing channel, as well as the effects of deuteration.

One primary motivation for the present direct dynamics study was as a means to search for the mechanism for formation of the $H_2 + HCO$ products. In particular, it was postulated that the configurations along the trajectories leading to $H_2 + HCO$ would provide useful starting geometries for the determination of the corresponding transition state. However, such re-optimizations have also failed to yield a transition state corresponding to the direct dissociation of methoxy into $H_2 + HCO$. Instead, they yield either the transition state for $H +$

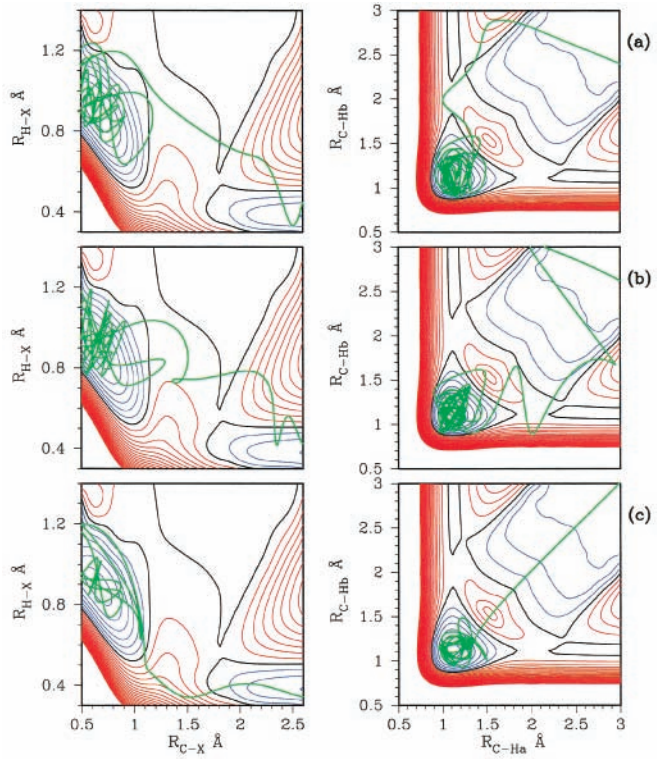

Figure 8. Two two-dimensional projections of each of three selected H_2-producing trajectories. The coordinates are the same as those defined in Figures 5 and 6. The black contours correspond to the saddle point for the reaction H + $H_2CO \rightarrow H_2$ + HCO. Blue contours are lower in energy. Red contours are higher.

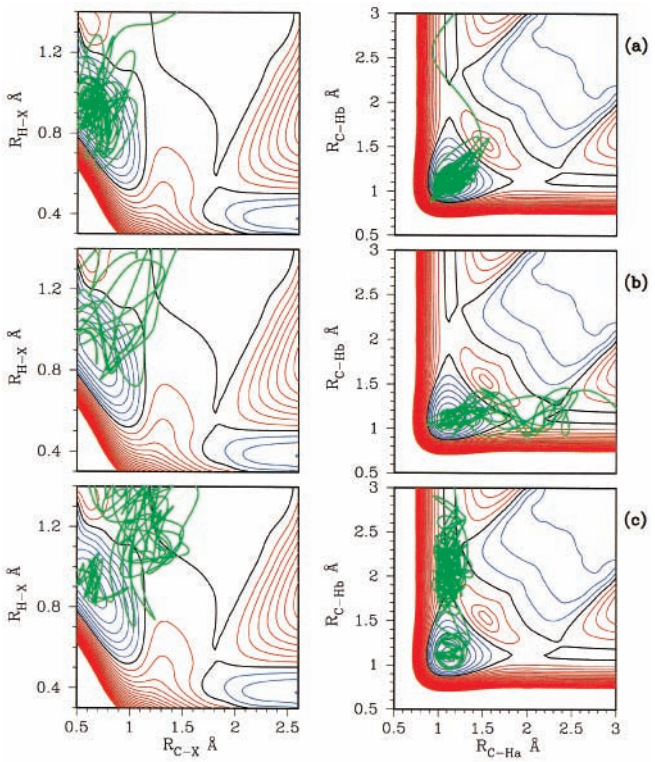

Figure 9. Two two-dimensional projections of each of three selected H-atom producing trajectories. The coordinates are the same as those defined in Figures 5 and 6.

$H_2CO \rightarrow H_2$ + HCO or the transition state for $H_3CO \rightarrow$ H + H_2CO. This failure to find a transition state for the direct elimination of H_2 from H_3CO offers further support to the conclusion that there is no saddle point for this process.

There is an interesting correlation between the potential energy surface for the present CH_3 + O system and that for the analogous H_2 + CN system, as can be seen via a comparison of the present Figure 6 with Figure 4 of ref 22. For the H_2 + CN reaction, there was also no saddlepoint directly connecting the reactants with the H_2CN complex. Instead, the ridge separating the potential well for the complex from the H_2 channel played an important role in the calculated dynamics, just as it does for the present reaction. The focus of ref 23 was on the H_2 + CN reaction and the presence of the ridge led to the H + HCN channel being the dominant channel for this reaction. Furthermore, this channel was found to arise via a direct abstraction, rather than via addition followed by elimination. In the dissociation direction of interest here, the ridge (cf. Figure 6) makes it difficult for the complex (CH_3O here) to directly produce the H_2 products, and it is the ultimate cause for the branching fraction being as small as it is.

For illustrative purposes, projections of sample trajectories onto the two-dimensional potential energy surface contour plots are provided in Figure 8 for some trajectories that produce H_2 + HCO and in Figure 9 for some trajectories that produce H + H_2CO. The trajectories illustrated in Figure 8a,b provide examples of cases where the dissociation effectively follows the minimum energy path. They first proceed over the barrier for producing H + H_2CO, then make their way over to the H + $H_2CO \rightarrow H_2$ + HCO saddle point region, and finally fall into the H_2 + HCO product well. Such trajectories might be termed frustrated H loss trajectories.

In the plots with two constrained CH distances (the right-hand panels), the H + $H_2CO \rightarrow H_2$ + HCO saddlepoint lies quite close to the valley corresponding to production of H + H_2CO. In those plots, the branching between H_2CO and HCO formation appears to be determined by whether the trajectory passes to the inside or outside of the H + $H_2CO \rightarrow H_2$ + HCO saddlepoint. Meanwhile, the left-hand panels provide a greater separation of the two saddle-point regions and appear to suggest that there is instead some dynamical effect hindering the dissociation into H + H_2CO.

One possibility is that the effective orbital barriers provide this hindering. Such effective barriers are exceptionally large for H-producing channels (due to the small mass and weak potential interactions for the H atom) and could be the cause of the abrupt turn in the trajectories (in Figure 8a,b) away from the H + H_2CO products shortly after passing the $CH_3O \rightarrow$ H + H_2CO saddle point. The magnitude of such barriers is greatly reduced for the H_2 + HCO channel, and so, the same trajectory has no difficulty proceeding on to the H_2 products. Interestingly, when averaged over all trajectories with $J = 50$, the orbital angular momentum for the H_2 + HCO products is 26 (evaluated at the end of the trajectory), which is indeed much greater than the value of 17 for the H + H_2CO products. Similarly, the range of calculated orbital angular momentum values extends to much higher values for the H_2 + HCO products (9−73) than those for the H + H_2CO products (1−47).

The trajectory illustrated in Figure 8c provides an example of an alternative dynamics that also produces H_2 + HCO. This trajectory proceeds directly over the ridge separating the CH_3O complex from H_2 + HCO. One aspect of trajectories such as this one, that essentially pass by the lower left of the H + $H_2CO \rightarrow H_2$ + HCO saddle point (in the left-hand panels), is that the product H_2 vibrational excitation tends to be much lower than that for those which pass directly through it or on the right-

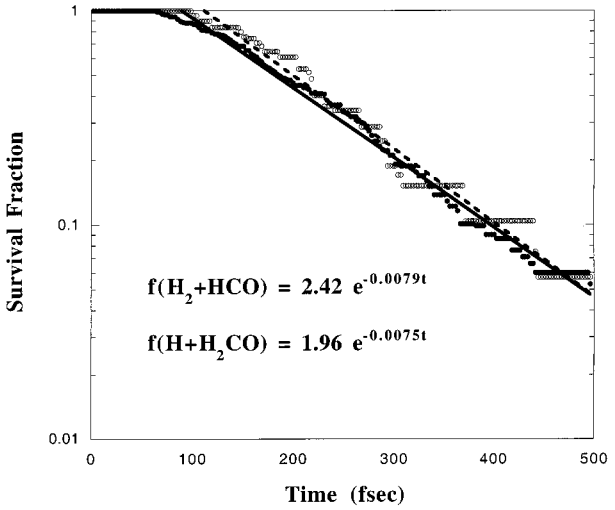

Figure 10. Logarithmic plot of the survival fractions as a function of time from the $CH_3 + O$, $J = 50$, trajectory calculations. Filled symbols and solid line are for the $H + H_2CO$ channel. Open symbols and dotted line are for the $H_2 + HCO$ channel.

hand side. The majority of the trajectories are more like that shown in Figure 8c than those shown in Figure 8a,b.

It is instructive to consider the shape of the curve describing the J dependence of the branching fraction. The initial rise in the branching ratio at low J may be correlated with an increasing effect of the orbital barriers. The average product orbital angular momentum for the $H + H_2CO$ products increases with total angular momentum J, which might lead to a greater number of frustrated H loss trajectories. The drop in the branching ratio at high J may instead indicate that the orbital barriers are no longer important, perhaps due to a shift of the transition state to quite short separations. Interestingly, for $J = 100$, none of the $H_2 +$ HCO forming trajectories appear to be frustrated H loss trajectories. Instead all proceed directly over the ridge. In contrast, for $J = 0$, nearly half of the H_2 is produced via the frustrated H loss mechanism.

The trajectory illustrated in Figure 9a is fairly typical of the trajectories that produce $H + H_2CO$. In particular, the trajectories tend to simply oscillate in the CH_3O well, occasionally experiencing quite large amplitude motion, until such a time as they pass over the $CH_3O \rightarrow H + H_2CO$ saddle point. From that point, the trajectories that produce $H + H_2CO$ proceed directly on to products.

Some trajectories do sample the H_2COH well as illustrated in Figure 9b,c, where the motion on the top left of the plots (for the left-hand panels) corresponds to a time when the trajectory is sampling the H_2COH well. In Figure 9b, this trajectory ultimately returns to the CH_3O well and then dissociates from there to $H + H_2CO$, while in Figure 9c, the trajectory directly dissociates from the H_2COH well. It is also energetically possible for the H_2COH well to dissociate to $H_2 +$ HOC and to isomerize to $HCOH_2$, but such channels are not observed. The transition states for these alternative channels are simply too high in energy to compete with the observed channels.

A plot of the surviving fraction of the reactive flux as a function of time is provided for the portion correlating with each product channel in Figure 10. This plot is for $CH_3 + O$ at $J = 50$. The time for decay of any one trajectory is simply taken as the time at which the trajectory is terminated due to the occurrence of a large interatomic distance. The absence of any decay for the first 50−100 fs in these plots is indicative of the time required to propagate from the initial entrance channel dividing surface into the complex region and on to the final termination point. The subsequent decay of these plots is more or less exponential with fitted decay constants of 7.5×10^{12} and 7.9×10^{12} s^{-1} for the $H + H_2CO$ and $H_2 + HCO$ channels, respectively.

If there is strong coupling between the two-phase space regions of the complex that correlate with dissociation into either $H + H_2CO$ or into $H_2 + HCO$, then the two dissociations occur in competition, but together. In this case, the time dependence of the $H + H_2CO$ products may be written as

$$\frac{dN_{H+H_2CO}}{dt} = k_{H+H_2CO}N_{CH_3O}(t) = k_{H+H_2CO}N_{CH_3O}(t=0)e^{-k_{tot}t}$$

where

$$k_{tot} = k_{H+H_2CO} + k_{H_2+HCO}$$

This implies then that

$$N_{H+H_2CO}(t) = N_{CH_3O}(t=0)[1 - e^{-k_{tot}t}]\frac{k_{H+H_2CO}}{k_{tot}}$$

A similar result applies to the $H_2 + HCO$ channel, and so, the fitted decay constants should be, and in essence are, identical. Interestingly, the decay constant is a factor of 10 smaller than the corresponding classical rigid-rotor harmonic-oscillator transition state theory (TST) estimate of 7×10^{13} for the $CH_3O \rightarrow H + H_2CO$ transition state. Thus, it appears that the decay of the CH_3O complex may be determined to some extent by the rate of energy transfer. However, it is worth noting that the use of a fixed transition state estimate and rigid-rotor harmonic-oscillator approximations may contribute significantly to the difference. An analogous transition state estimate cannot be made for the $H_2 + HCO$ channel due to the apparent absence of a saddle point.

Interestingly, the quantum TST estimate is within a factor of 2 of the classical estimate, due once again to the large exothermicity of the reaction. This is also true of the statistical estimates for the $CH_3O \leftrightarrow H_2COH$ isomerization rates and for the reactive flux through the $H + H_2CO \rightarrow H_2 + HCO$ saddle point. This near-equivalence of the quantum and classical TST estimates validates to some extent the present use of classical dynamics.

Conclusions

The results of both the experimental and theoretical studies reported here confirm the existence of a CO producing channel in the reaction of CH_3 with O atoms. The mechanism involves the elimination of H_2 from an energy-rich CH_3O radical forming HCO, followed by the decomposition of HCO to form the observed CO (v) product. The most unusual feature of this mechanism is that there appears to be no saddle point for the direct elimination of H_2 from CH_3O. The methoxy radical is formed with ~90 kcal/mol of excess energy, or ~60 kcal/mol above its lowest barrier for decomposition (CH bond cleavage). At these high energies, trajectories are found to stray far from the minimum-energy paths, resulting in the unexpected products. Experiment and theory agree that the importance of the CO (v) product channel is noticeably diminished in the $CD_3 + O$ reaction relative to in the $CH_3 + O$. Theory also predicts that

this branching ratio is nearly independent of temperature, perhaps decreasing by 0.02 from room temperature up to 1000 K.

Acknowledgment. This work was supported by the U. S. Department of Energy, Office of Basic Energy Sciences, Division of Chemical Sciences, Geosciences, and Biosciences. The DOE Contracts are W-31-109-ENG-38 (Argonne) and DE-FG03-94ER 14433 (University of Colorado). In addition, the researchers at the University of Colorado gratefully acknowledges additional equipment provided by the National Science Foundation. D.E.H. is grateful to JILA for the award of a Visiting Fellowship.

References and Notes

(1) Seakins. P. W.; Leone, S. R. *J. Phys. Chem.* **1992**, *96*, 6**,** 4478.

(2) Fockenberg, C.; Hall, G. E.; Preses, J. M.; Sears, T. J.; Muckerman, J. T. *J. Phys. Chem. A* **1999**, *103*, 5722.

(3) Preses, J. M.; Fockenberg, C.; Flynn, G. W. *J. Phys. Chem. A* **2000**,*104*, 6758.

(4) Min, Z.; Quandt, R. W.; Wong, T.-H.; Bersohn, R. J. *J. Chem. Phys*. **1999**,*21*, 411

(5) Leone, S. R.; *Acc. Chem. Res.* **1989**, *22***,** 139.

(6) Rogers, S. A.; Leone, S. R. *Appl. Spectrosc.* **1993**, *47***,** 1430.

(7) Sloan, J. J. *Advances in Spectroscopy*; Wiley: New York, 1989; Vol. 18.

(8) Reid, J. P.; Qian, C. X. W.; Leone, S. R. *Phys. Chem. Chem. Phys.* **2000**, *4*, 853.

(9) Hancock, G.; Heard, D. E. In *Advances in Photochemistry*; Volman, D.H., Hammond, G. S., Neckers D. C., Eds.; Wiley: New York, 1993; Vol. 18, pp 1−65.

(10) Rudolph, R. N.; Hall, G. E.; Sears, T. J. *J. Chem. Phys.* **1996**, *105***,** 7889.

(11) Frisch, M. J.; Trucks, G. W.; Schlegel, H. B.; Scuseria, G. E.; Robb, M. A.; Cheeseman, J. R.; Zakrzewski, V. G.; Petersson, G. A.; Montgomery, J. A., Jr.; Stratmann, R. E.; Burant, J. C.; Dapprich, S.; Millam, J. M.; Daniels, A. D.; Kudin, K. N.; Strain, M. C.; Farkas, O.; Tomasi, J.; Barone, V.; Cossi, M.; Cammi, R.; Mennucci, B.; Pomelli, C.; Adamo, C.; Clifford, S.; Ochterski, J.; Petersson, G. A.; Ayala, P. Y.; Cui, Q.; Morokuma, K.; Malick, D. K.; Rabuck, A. D.; Raghavachari, K..; Foresman, J. B.; Cioslowski, J.; Ortiz, J. V.; Stefanov, B. B.; Liu, G.; Liashenko, A.; Piskorz, P.; Komaroni, I.; Gomperts, R.; Martin, R. L.; Fox, D. J.; Keith, T. A.; Al-Laham, M. A.; Peng, C. Y.; Nanayakkara, A.; Gonzalez, C.; Challacombe, M.; Gill, P. M. W.; Johnson, B. G.; Chen, W.; Wong, M. W.; Andreas, J. L.; Head-Gordon, M.; Replogle, E. S.; Pople, J. A. *Gaussian 98*; Gaussian, Inc.: Pittsburgh, PA, 1998.

(12) Knowles, P. J.; Hampel, C.; Werner, H.-J. *J. Chem. Phys.* **1993**, *99*, 5219.

(13) MOLPRO is a package of ab initio programs written by Werner, H.-J.; Knowles, P. J., with contributions from Almlof, J.; Amos, R. D.; Berning, A.; Cooper, D. L.; Deegan, M. J. O.; Dobbyn, A. J.; Eckert, F.; Elbert, S. T.; Hampel, C.; Lindh, R.; Lloyd, A. W.; Meyer, W. Nicklass, A.; Peterson, K.; Pitzer, R.; Stone, A. J.; Taylor, P. R.; Mura, M. E.; Pulay, P.; Schutz, M.; Stoll, H.; Thorsteinsson, T..

(14) Dunning, T. H., Jr. *J. Chem. Phys.*, **1989**, *90*, 1007.

(15) Kendall, R. A.; Dunning, T. H., Jr.; Harrison, R. J. *J. Chem. Phys.*, **1992**, *96*, 6796.

(16) Woon, D. E.; Dunning, T. H., Jr. *J. Chem. Phys.*, **1993**, *98*, 1358.

(17) Walch, S. P. *J. Chem. Phys.*, **1993**, *98*, 3076.

(18) Forsythe, K. M.; Gray, S. K.; Klippenstein, S. J.; Hall, G. E. *J. Chem. Phys.* **2001**, *115*, 2134.

(19) Klippenstein, S. J. *J. Phys. Chem.*, **1994**, *98*, 11459.

(20) Tuckerman, M.; Berne, B. J.; Martyna, G. J. *J. Chem. Phys.*, **1992**, *97*, 1990.

(21) Gray, S. K.; Noid, D. W.; Sumpter, B. G. *J. Chem. Phys.* **1994**, *101*, 4062.

(22) Atkinson, R.; Baulch, D. L.; Cox, R. A.; Hampson, R. F.; Kerr, J. A.; Troe, J. *J. Phys. Chem. Ref. Data* **1994**, *23*, 847.

(23) ter Horst, M. A.; Schatz, G. C.; Harding, L. B. *J. Chem. Phys.* **1996**, *105*, 558.